World Scientific
www.worldscientific.com

OVERVIEW ON DIRECT AND INDIRECT MEASUREMENTS
OF COSMIC RAYS
Some thoughts on galactic cosmic rays and the knee

JÖRG R. HÖRANDEL

University of Karlsruhe, Institut für Experimentelle Kernphysik, PO 3640, Karlsruhe, D-76021 Germany
hoerandel@ik.fzk.de

An overview is given on results from direct and indirect measurements of galactic cosmic rays. Their implications on the contemporary understanding of the origin of cosmic rays and the knee in their energy spectrum are discussed.

Keywords: Cosmic rays; energy spectrum; mass composition; sources; propagation; knee

1. INTRODUCTION

Cosmic rays (CRs) in the energy range from several GeV up to about 100 PeV are assumed to be mostly of galactic origin. At energies up to several 100 MeV individual isotopes can be identified, e.g. with the ACE/CRIS experiment,[1] a satellite borne silicon detector telescope. At higher energies, CRs are identified by their charge and the energy measurement becomes an experimental challenge. Various techniques are utilized, like the determination of the particles momenta in magnet spectrometers (e.g. BESS,[2]) the (partial) absorption of nuclei in calorimeters (e.g. ATIC,[3]) or the measurement of transition radiation emitted by relativistic particles (e.g. TRACER[4]). Circumpolar long duration balloon flights offer the possibility of a long exposure (≥ 14 d) combined with low atmospheric overburden (typically < 5 g/cm^2) as recently demonstrated by the ATIC,[5] TIGER[6] and TRACER[7] experiments.

At energies above 1 PeV the steeply falling spectrum requires large detection areas (exceeding several 10^4 m^2) and exposure times of several years, which presently can be realized only in ground based installations. They measure the secondary products generated by the CR particles in the atmosphere – the extensive air showers. The challenge of these investigations is to reveal the properties of the primary particle behind an absorber – the atmosphere – with a total thickness, corresponding to 11 hadronic interaction lengths or 30 radiation lengths. Consequently, these experiments have a coarser resolution and only mass groups or the average primary mass are derived. Two basic approaches can be distinguished: Measuring the debris of the particle cascade at ground level by registering the

main shower components, the electromagnetic, muonic, and hadronic parts. Or measuring the longitudinal shower development in the atmosphere, exploring the Čerenkov or fluorescence light generated predominantly by the shower electrons. Examples are the KASCADE[8]-Grande[9] or EAS-TOP[10] installations, measuring simultaneously the electromagnetic, muonic, and hadronic shower components, the SPASE[11]/AMANDA[12] experiment, investigating electrons and high energy muons, or the BLANCA[13] Čerenkov detector.

In this article an overview on results from direct and indirect measurements is given, concerning the sources of CRs (§2), their propagation through the Galaxy (§3), and the energy spectra and mass composition observed at Earth (§4). Their implications on the understanding of the origin of the knee are discussed (§5).

2. SOURCES OF COSMIC RAYS

A big step towards the understanding of CR sources would be their direct observation in the sky. However, charged CRs are deflected in the galactic magnetic fields, the gyromagnetic radius of a proton with an energy of 1 PeV is about 0.4 pc. But γ-rays are good candidates for a point source search. Photon emission of supernova remnants (SNRs) has been detected in a wide energy range from radio wave lengths to x-rays. The observations are interpreted as synchrotron emission from electrons, which are accelerated in these regions.[14] The HEGRA experiment[15] has detected an excess of γ-rays with TeV energies from the SNR Cassiopeia A. This is interpreted as evidence for hadron acceleration in the SNR. The hadrons interact with protons of the interstellar medium close to the source region, producing π^0s, which decay into high-energy photons. The flux is compatible with a model of electron and hadron acceleration in shock fronts of the SNR.[14]

Despite of the above-mentioned deflection, it is of great interest to study the arrival direction of charged CRs as well. The result of such an analysis from the KASCADE experiment[16] is depicted in Fig. 1 (*left*). Shown is the distribution of the significances from a sky map of the arrival direction of showers with energies above 0.3 PeV covering a region from $10°$ to $80°$ in declination. For an isotropic distribution the significances are expected to follow a Gaussian distribution as indicated by the solid line. Results for all events are presented, as well as for a selection of muon-poor showers. The latter are expected from potential primary γ-rays. No significant deviation of the data from the Gaussian distribution can be recognized. The analysis has been deepened by investigating a narrow band ($\pm 1.5°$) around the galactic plane. Also circular regions around SNRs and TeV-γ-ray sources have been studied. None of the searches provided a hint for a point source. In addition, no clustering of the arrival direction for showers with primary energies above 80 PeV is visible. Claims by the MAKET-ANI experiment for a point-source detection[17] have been withdrawn meanwhile.[18]

Despite no sources have been detected with charged particles, information on the composition at the source can be obtained from measurements of the abundance of refractory nuclei. They appear to have undergone minimal elemental fractionation relative to one another. The derived abundance at the source is presented in Fig. 1 (*right*) versus the abundance in the solar system.[19] The two samples exhibit an extreme similarity over a wide
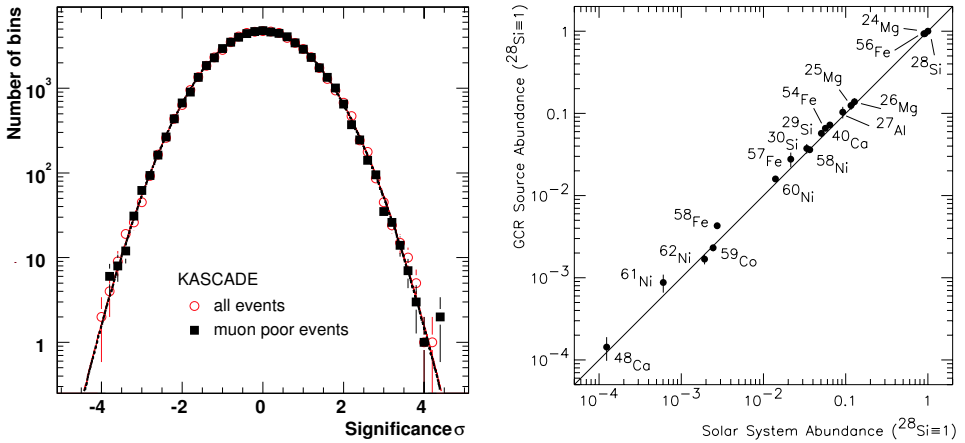
Fig. 1.   *Left*: Distribution of the significance values from a sky map of the arrival direction of CRs as measured by the KASCADE experiment[16] for the complete data set (open circles) and a selection of muon poor showers (filled squares). *Right*: Comparison of derived CR source abundances of refractory nuclides with solar-system abundances according to measurements with ACE/CRIS[19] normalized to ^{28}Si.

range. Of the 18 nuclides included in this comparison, only ^{58}Fe is found to have an abundance relative to ^{28}Si that differs by more than a factor of 1.5 from the solar-system value. When uncertainties are taken into account, all of the other abundances are consistent with being within 20% of the solar values. This indicates that CRs are accelerated out of a sample of well mixed interstellar matter.

Motivated by the observations, it is assumed that at least a large fraction of CRs are accelerated in supernova remnants.[20–23] However, recent progress in the understanding of γ-ray bursts has put forward the idea that a subsample of high-energy CRs may be accelerated in γ-ray bursts.[24, 25]

3. PROPAGATION OF COSMIC RAYS

After acceleration, the particles propagate in a diffusive process through the Galaxy, being deflected many times by the randomly oriented magnetic fields ($B \sim 3 \ \mu$G). The nuclei are not confined to the galactic disc, they propagate in the galactic halo as well. The diffuse γ-ray background, extending well above the disc, detected by the EGRET experiment, exhibits a structure in the GeV region, which is interpreted as indication for the interaction of propagating CRs with interstellar matter.[26] The height of the halo has been estimated with measurements of the ^{10}Be/^{9}Be-ratio by the ISOMAX experiment[27] to be a few kpc. The measured abundance of radioactive nuclei in CRs with the CRIS instrument yields a residence time in the Galaxy of about 15×10^6 a for particles with GeV energies.[28]

Information on the propagation pathlength of CRs is often derived from the measurement of the ratio of primary to secondary nuclei. The latter are produced through spallation during propagation in the Galaxy. As an example, the measured boron-to-carbon ratio is shown in Fig. 2 (*left*) as function of energy.[29] The energy dependence of the measured ratio
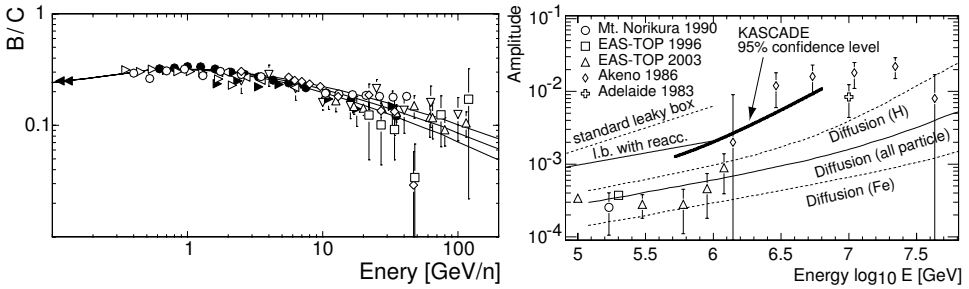
Fig. 2. *Left*: Measured boron-to-carbon ratio as function of energy, the lines indicate model predictions, see Ref. 29. *Right*: Rayleigh amplitudes as function of energy for various experiments, for references see 30. Additionally, model predictions for Leaky Box models[31] and a diffusion model[32] are shown. For the latter, the lines indicate the expected anisotropy for primary protons, iron nuclei, and all particles.

is frequently explained in Leaky Box models by a decrease of the pathlength of CRs in the Galaxy $\Lambda(R) = \Lambda_0 (R/R_0)^{-\delta}$, with typical values $\Lambda_0 \approx 10 - 15$ g/cm^2, $\delta \approx 0.5 - 0.6$, and the rigidity $R_0 \approx 4$ GV.

At higher energies such measurements are not feasible due to the limited mass resolution of air shower experiments. However, at these energies the large scale anisotropy is expected to reveal properties of the CR propagation. The Rayleigh formalism is applied to the right ascension distribution of extensive air showers measured by KASCADE.[30] No hints of anisotropy are visible in the right ascension distributions in the energy range from 0.7 to 6 PeV. This accounts for all showers, as well as for subsets containing showers induced by predominantly light or heavy primary nuclei. Upper limits are shown together with results from other experiments in Fig. 2 (*right*). It presents the Rayleigh amplitude as a function of energy. The experimental results are compared to the anisotropy expected from calculations of the propagation of CRs in the Galaxy. The data reflect a trend predicted by a diffusion model.[32] This indicates that leakage from the Galaxy and consequently a decreasing pathlength $\Lambda(E)$ plays an important part during CR propagation at high energies and most likely, also for the origin of the knee.

Leaky Box models are successful at GeV energies as discussed above. In the PeV regime, however, they seem to be faced with some difficulties. Two versions of a Leaky Box model,[33] with and without reacceleration, seem to be ruled out by the anisotropy measurements, see Fig. 2. This relates to the extremely steep decrease of the pathlength $\Lambda \propto E^{-0.6}$, yielding at PeV energies unrealistically small values for Λ. Even for a residual pathlength model,[34] at 1 PeV the pathlength would be smaller than the matter traversed along a straight line from the center of the Galaxy to the solar system.[35]

4. ENERGY SPECTRA AND MASS COMPOSITION

At energies below 100 TeV the energy spectra of individual elements have been measured with detectors above the atmosphere. Examples for protons, helium and iron nuclei are compiled in Fig. 3. The measured spectra can be described by power laws. For the iron

spectrum at low energies the modulation due to the magnetic fields of the heliosphere causes the flux suppression. Actual experiments, like ATIC[5] and TRACER,[7] as well as the proposed ACCESS[41] space project are expected to improve the experimental situation in the region around 0.1 to 1 PeV, where large uncertainties are visible in the figure. More precise fluxes in this region would be valuable to intercalibrate air shower measurements.

The elemental abundance at 1 TeV is presented in Fig. 4 (*left*) as function of nuclear charge number for elements up to nickel. The experimental status for the heavier elements is summarized in Fig. 4 (*right*). All stable elements of the periodic table have been registered in CRs. In both panels the CR abundance is compared to the abundance in the solar system[42] normalized to silicon and iron, respectively. The overall similarity of the two samples of matter, already seen in Fig. 1, is reflected here on a coarser scale.

At higher energies, many air shower experiments have reported fluxes for all particles. A compilation is presented in Fig. 5 (*left*). The energy scale of the individual experiments has been slightly normalized ($\pm 10\%$) in order to match the flux with that obtained by direct measurements.[36] A good agreement between the experiments in the reconstructed shape of the spectrum is evident. The knee at ~ 4.5 PeV is visible and there is indication for a smaller structure at ~ 400 PeV, the second knee.
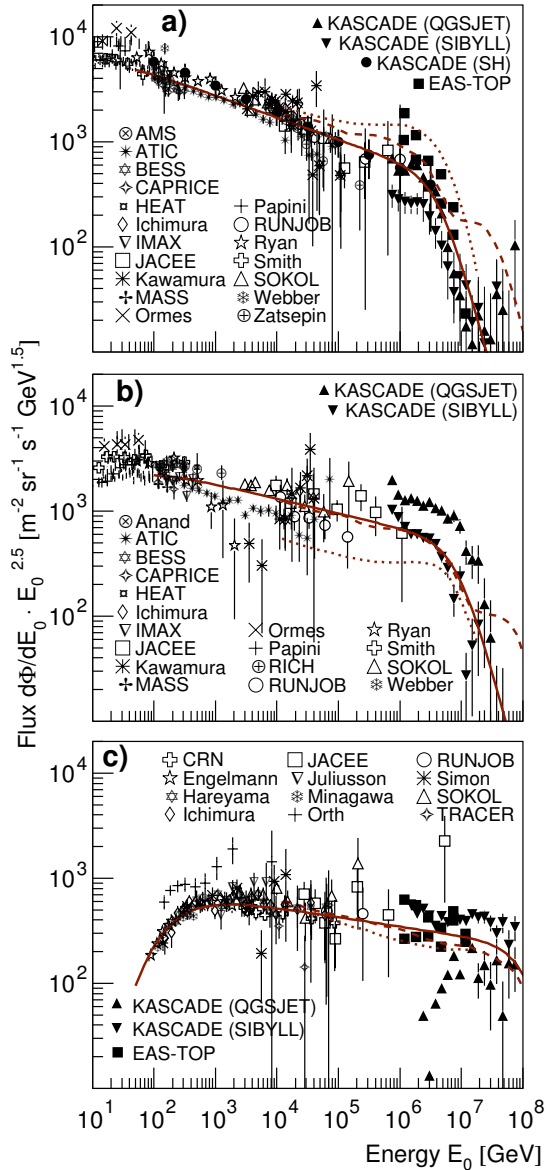

Fig. 3. Energy spectra for elemental groups **a)** protons, **b)** helium, and **c)** iron. Open symbols give results of direct measurements, for references see 36, 4, 5. Filled symbols represent data from air shower measurements: KASCADE electrons/muons interpreted with two interaction models[37] (preliminary), KASCADE single hadrons[38] and EAS-Top electrons/muons.[39] The data are compared to calculations by Kalmykov *et al.*[40] ($\cdots$), Sveshnikova[23] (- - -), and the Poly-Gonato model[36] (—).
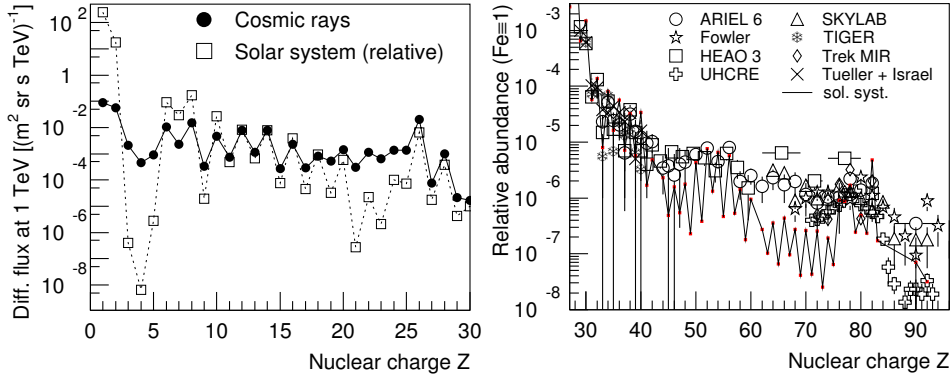
Fig. 4.   *Left*: Abundance of elements ($Z \leq 28$) in CRs[36,43] at 1 TeV. *Right*: Relative abundance of CR elements ($Z > 28$) normalized to Fe$\equiv$ 1 from various experiments around 1 GeV/n. For references see 36, 6. For comparison, abundances in the solar system[42] are presented as well, normalized to Si (*left*) and to Fe (*right*).

Most valuable to reveal the origin of the knee are measurements of the energy spectra for individual elements or at least mass groups. KASCADE studied the influence of different hadronic interaction models used in the simulations to interpret the data.[37] Two sets of spectra, derived from the observation of the electromagnetic and muonic air shower components, applying an unfolding procedure based on the Gold algorithm and using COR-SIKA[44] with the hadronic interaction models QGSJET and SIBYLL are compiled in Fig. 3 for three elemental groups. As can be seen in the figure, the fluxes depend on the model used. KASCADE emphasizes that, at present, there are systematic differences between measured and simulated observables which cause the ambiguities of the spectra. These conclusions apply in a similar way also to other experiments. A correct deconvolution of energy spectra requires a more precise knowledge of the hadronic interactions.

Fig. 3 also shows the spectrum of primary protons, which has been derived from the flux of unaccompanied hadrons measured by KASCADE.[38] The spectrum is compatible with the proton flux as obtained from the unfolding procedure when using the QGSJET model. The EAS-TOP experiment published two sets of spectra with different assumptions about the contribution of protons and helium nuclei derived from the measurements of the electromagnetic and muonic shower components.[39] The resulting fluxes are indicated by two squares per primary energy. To guide the eye, the solid lines indicate power law spectra with a cut-off at $Z \times 4.5$ PeV.

The dashed lines represent calculations of energy spectra for nuclei accelerated in supernovae.[23] It is assumed that the particles are accelerated in a variety of supernovae populations, each having an individual maximum energy that can be attained during acceleration, which results in the bumpy structure of the obtained spectra. The dotted lines reflect calculations of the diffusive propagation of particles through the Galaxy.[40] The leakage of particles yields a rigidity dependent cut-off. Comparison with the data may suggest a *qualitative* understanding of the energy spectra. However, for a precise *quantitative* understanding, detailed investigations of the systematic errors of the measurements are necessary and the description of the interaction processes in the atmosphere needs to be improved.
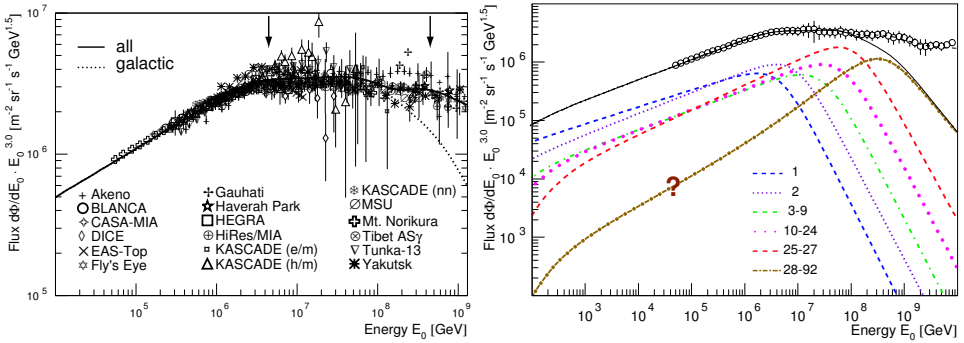
Fig. 5. *Left*: Normalized all-particle energy spectra from different experiments. The lines indicate the average all particle spectrum and the contribution of galactic CRs. The knee at $E_k \sim 4.5$ PeV and the second knee at ~ 400 PeV$\approx 92 \cdot E_k$ are indicated. *Right*: The average flux of the measurements (*left*) is represented by the data points. Additionally, spectra for elemental groups with the indicated charge number range according to a parameterization of the measurements are depicted, including a proposed contribution of ultra-heavy elements ($Z > 28$), extrapolated from measurements at GeV energies ("?"). For details and references see 36.

While the elemental abundance is relatively well known at low energies from direct measurements (see Fig. 4), at higher energies, air-shower experiments provide information on mass groups or on the average mass. Frequently, the mean logarithmic mass $\langle \ln A \rangle$, defined as $\langle \ln A \rangle = \sum r_i \ln A_i$, where r_i is the relative fraction of nuclei with atomic mass number A_i, is used to characterize the composition. $\langle \ln A \rangle$ is often derived from the ratio of particles measured at ground level. For a primary proton more electrons and hadrons and fewer muons are registered as compared to an iron induced shower with the same energy. The data from many experiments are compiled in Fig. 6 (*left*). They exhibit an increase of $\langle \ln A \rangle$ as function of energy in the knee region. The increase is compatible with expectations, assuming a cut-off behavior of the flux of individual elements as indicated in Fig. 3 by the solid line. The second class of experiments reconstructs the average depth of the shower maximum $X_{\max}$ from the observation of Čerenkov and fluorescence light. Using the model QGSJET to derive the mean logarithmic mass from the data results in a light mass composition at high energies in contradiction to the findings just mentioned.[36] Introducing modifications to QGSJET, namely lowering the inelastic cross sections and slightly increasing the elasticity of hadronic interactions, this discrepancy can be reduced[45] and the mean logarithmic mass rises as function of energy, see Fig. 6 (*right*).

The average experimental values from both classes of air shower measurements presented in Fig. 6 are shown as light grey area in Fig. 7. It represents the mean value ± 1 standard deviation. The dark grey area represents the results of direct measurements above the atmosphere. This experimental situation will be compared to predictions of various models in the next section.

A different interpretation of the experimental results is given in Fig. 5 (*right*). The average of the flux values shown in the left panel is displayed by the data points. The spectra for elemental groups are presented according to a parameterization of the measurements,[36] which corresponds to the solid lines in Figs. 3 and 6, where the agreement with the data has
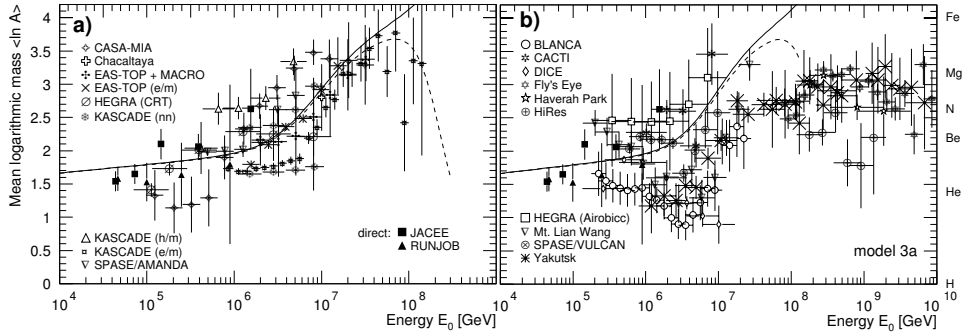
Fig. 6.   Mean logarithmic mass of CRs reconstructed from **a)** experiments measuring electrons, muons, and hadrons at ground level[36,46–48] and **b)** observations of the shower maximum interpreted with a modification of QGSJET.[45] The lines indicate expectations according to the Poly Gonato model.[36]

been discussed. Also shown is a proposed contribution of ultra-heavy elements ($Z > 28$), extrapolated from measurements at GeV energies. The individual spectra exhibit a cut-off at $E_Z = Z \cdot 4.5$ PeV. The cut-off for the heaviest elements agrees with the energy of the second knee at ~ 400 PeV, which is interpreted as the end of the galactic CRs, while the knee is caused by the cut-off of the light elements. The sum spectrum of all elements is given by the solid line, which fits nicely the average measured spectrum up to 100 PeV. At low energies where the nuclei traverse a large amount of matter (~ 10 g/cm^2), heavy nuclei are more likely to interact with the interstellar matter as compared to light elements ($\sigma_{inel} \propto A^{2/3}$) and the spectra observed at earth are expected to be slightly flatter for heavy nuclei. At the respective knees Λ is less than 1 g/cm^2, thus for the heaviest elements around 400 PeV more than 40% of the nuclei are expected to survive without interaction.[35]

5. THE KNEE IN THE ENERGY SPECTRUM

The bulk of CRs is assumed to be accelerated in strong shock fronts of SNRs.[58] The finite lifetime of a shock front ($\sim 10^5$ a) limits the maximum energy attainable for particles with charge Z to $E_{max} \sim Z \cdot (0.1 - 5)$ PeV. Many versions of this scenario have been discussed.[20–23] The models differ in assumptions of properties of the SNRs like magnetic field strength, available energy etc. This yields differences in $\langle \ln A \rangle$, as can be inferred from Fig. 7a. While older models[21] limit the maximum energy to about 0.1 PeV, recent ideas,[23] taking into account latest observations of SNRs, predict maximum energies above 1 PeV. In such a model sufficient energy is released from SNRs to explain the observed spectra, see in Fig. 3 the calculations by Sveshnikova *et al.* A special case of SNR acceleration is the single source model,[50] which predicts in the knee region pronounced structures in the all-particle energy spectrum, caused by a single SNR. Such structures can not be seen in the compilation of Fig. 5.

In the literature also other acceleration mechanisms, like the acceleration of particles in γ-ray bursts, are discussed.[24,25,49] They differ in their interpretation of the origin for the knee. The approach by Plaga, assuming Fermi acceleration in a "cannon ball" is not
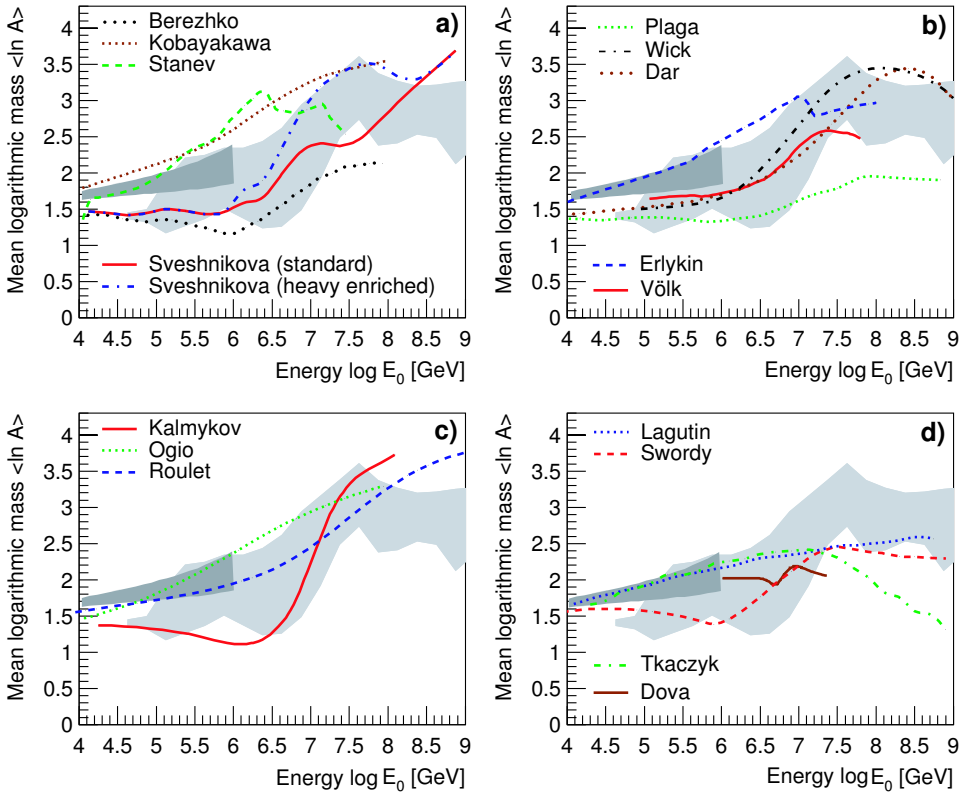
Fig. 7. Mean logarithmic mass as function of energy obtained by direct observations (dark grey area) and air shower experiments (light grey area) compared with different models (lines). **a)** Acceleration in SNRs;[20–23] **b)** acceleration in GRBs,[24,25,49] single source model,[50] reacceleration in the galactic wind;[51] **c)** diffusion in Galaxy;[40,52,53] **d)** propagation in the Galaxy,[34,54] as well as interaction with background photons[55] and neutrinos.[56] For details see Ref. 57.

compatible with the measured $\langle \ln A \rangle$ values, see Fig. 7b. A different interpretation of acceleration in the cannon ball model yields – at the source – a cut-off for individual elements proportional to their mass due to effects of relativistic beaming in jets. The predictions of the actual model are compatible with recent data.[25] However, it remains to be clarified how a detailed consideration of the propagation processes, e.g., in a diffusion model, effects the cut-off behavior observed at earth. Gamma-ray bursts as a special case of supernova explosions are proposed[24] to accelerate CRs from 0.1 PeV up to the highest energies ($> 10^{20}$ eV). In this approach the propagation of CRs is taken into account and the knee is caused by leakage from the Galaxy leading to a rigidity dependent cut-off behavior.

The propagation is accompanied by leakage of particles from the Galaxy. With increasing energy it becomes more and more difficult to confine the nuclei to the Galaxy. As mentioned above, the pathlength decreases as $\Lambda \propto E^{-\delta}$. Such a decrease will ultimately lead to a complete loss of the particles, with a rigidity dependent cut-off of the flux for individual elements. Many approaches have been undertaken to describe the propagation

process.[33,34,52-54] The Leaky Box model[34] and the anomalous diffusion model[54] yield cut-offs significantly weaker than the data shown in Fig. 3 (see Ref. 57).

The propagation as described in diffusion models[40,52,53] yields $\langle \ln A \rangle$-values which are presented in Fig. 7c. The models are based on the same principal idea,[33] but take into account different assumptions on details of the propagation process, like the structure of galactic magnetic fields etc. This results in a more or less strong cut-off for the flux at the individual knees and, accordingly, in a more or less strong increase of $\langle \ln A \rangle$. The model by Kalmykov *et al.*[40] has been used to describe the observed spectra in Fig. 3.

During the propagation phase, reacceleration of particles has been suggested at shock fronts in the galactic wind.[51] Also this mechanism yields a rigidity dependent cut-off.

Another hypothetical explanation for the knee are interactions of CRs with background particles like massive neutrinos[56,59] or photo disintegration in dense photon fields.[55,60] Such models appear to be excluded with a high level of confidence. The interactions would produce a large amount of secondary protons, which results in a light mass composition at high energies, not observed by the experiments, see Fig. 7d. Furthermore, a massive neutrino, proposed in Refs.[56,59] can be excluded by measurements of the WMAP and 2dFGRS experiments.[61]

A completely different reason for the knee is the idea to transfer energy in nucleon-nucleon interactions into particles, like gravitons[62] or extremely high-energy muons,[63] which are not observable (or not yet observed) in air shower experiments. The latter proposal seems to be excluded by recent measurements of the Baikal experiment[64] setting upper limits for the flux of muons above 10^5 GeV.

6. CONCLUSION

During the last decade significant progress has been made in the measurement of galactic CRs. Summarizing the large number of experimental observations, there are indications for a standard picture. At least a large fraction of CRs seems to be accelerated in supernova remnants up to energies of $Z \cdot (0.1 - 5)$ PeV. Higher energies may be reached in additional sources, such as γ-ray bursts. The elemental composition of the accelerated material is extremely similar to that in the solar system. The particles propagate in a diffusive process through the Galaxy. With rising energy the pathlength decreases and the particles escape easier from the Galaxy. This brings about the knee in the energy spectrum. The general shape of the energy spectra should be determined by the propagation process, maybe slightly modulated by properties of the source spectra.

References

1. E. C. Stone *et al.*, *Space Sci. Rev.* **86**, 357 (1998).
2. Y. Ajima *et al.*, *Nucl. Instrum. Meth.* **A443**, 71 (2000).
3. T. G. Guzik *et al.*, *Adv. Space Res.* **33**, 1763 (2004).
4. F. Gahbauer *et al.*, *Astrophys. J.* **607**, 333 (2004).
5. H. S. Ahn *et al.*, in *Proc. 28th Int. Cosmic Ray Conf., Tsukuba* **4**, 1833 (2003).
6. J. T. Link *et al.*, in *Proc. 28th Int. Cosmic Ray Conf., Tsukuba* **4**, 1781 (2003).
7. J. R. Hörandel, *Adv. Space Res.*, in press (2005).
8. T. Antoni *et al.*, *Nucl. Instrum. Meth.* **A513**, 490 (2003).
9. G. Navarra *et al.*, *Nucl. Instrum. Meth.* **A518**, 207 (2004).
10. M. Aglietta *et al.*, *Nucl. Instrum. Meth.* **A336**, 310 (1993).
11. J. E. Dickinson *et al.*, *Nucl. Instrum. Meth.* **A440**, 95 (2000).
12. E. Andres *et al.*, *Astropart. Phys.* **13**, 1 (2000).
13. J. W. Fowler *et al.*, *Astropart. Phys.* **15**, 49 (2001).
14. E. G. Berezhko *et al.*, *Astron. Astrophys.* **400**, 971 (2003).
15. F. Aharonian *et al.*, *Astron. Astrophys.* **370**, 112 (2001).
16. T. Antoni *et al.*, *Astrophys. J.* **608**, 865 (2004).
17. A. Chilingarian *et al.*, *Astrophys. J.* **597**, L129 (2003).
18. A. Chilingarian, private communication (2004).
19. M. Wiedenbeck *et al.*, in *Proc. 28th Int. Cosmic Ray Conf., Tsukuba* **4**, 1899 (2003).
20. E. G. Berezhko *et al.*, *Sov. Phys. JETP* **89**, 391 (1999).
21. T. Stanev *et al.*, *Astron. Astrophys.* **274**, 902 (1993).
22. K. Kobayakawa *et al.*, *Phys. Rev.* **D66**, 083004 (2002).
23. L. G. Sveshnikova *et al.*, *Astron. Astrophys.* **409**, 799 (2003).
24. S. D. Wick *et al.*, *Astropart. Phys.* **21**, 125 (2004).
25. A. Dar, preprint astro-ph/0408310 (2004).
26. A. W. Strong and I. V. Moskalenko, preprint astro-ph/9903370 (1999).
27. A. Molnar and M. Simon, in *Proc. 28th Int. Cosmic Ray Conf., Tsukuba* **4**, 1937 (2003).
28. N. E. Yanasak *et al.*, *Astrophys. J.* **563**, 768 (2001).
29. S. A. Stephens and R. E. Streitmatter, *Astrophys. J.* **505**, 266 (1998).
30. T. Antoni *et al.*, *Astrophys. J.* **604**, 687 (2004).
31. V. S. Ptuskin, *Adv. Space Res.* **19**, 697 (1997).
32. J. Candia *et al.*, *JCAP* **5**, 3 (2003).
33. S. V. Ptuskin *et al.*, *Astron. Astrophys.* **268**, 726 (1993).
34. S. P. Swordy, in *Proc. 24th Int. Cosmic Ray Conf., Rome* **2**, 697 (1995).
35. J. R. Hörandel *et al.*, *Int. J. Mod. Phys. A*, in press (2005).
36. J. R. Hörandel, *Astropart. Phys.* **19**, 193 (2003).
37. H. Ulrich *et al.*, *Eur. Phys. J.* **C33**, S944 (2004).
38. T. Antoni *et al.*, *Astrophys. J.* **612**, 914 (2004).
39. M. Aglietta *et al.*, *Astropart. Phys.* **21**, 583 (2004).
40. N. N. Kalmykov *et al.*, in *Proc. 26th Int. Cosmic Ray Conf., Salt Lake City* **4**, 263 (1999).
41. M. Israel *et al.*, *ACCESS: A Cosmic Journey (Formulation Study Report of the NASA ACCESS Working Group)* (2000).
42. A. G. W. Cameron, *Space Sci. Rev.* **15**, 121 (1973).
43. B. Wiebel-Soth *et al.*, *Astron. Astrophys.* **330**, 389 (1998).
44. D. Heck *et al.*, Report FZKA 6019, Forschungszentrum Karlsruhe (1998).
45. J. R. Hörandel, *J. Phys. G: Nucl. Part. Phys.* **29**, 2439 (2002).
46. M. Aglietta *et al.*, *Astropart. Phys.* **21**, 583 (2004).
47. M. Aglietta *et al.*, *Astropart. Phys.* **20**, 641 (2004).
48. K. Rawlins *et al.*, in *Proc. 28th Int. Cosmic Ray Conf., Tsukuba* **1**, 173 (2003).

49. R. Plaga, *New Astron.* **7**, 317 (2002).
50. A. D. Erlykin and A. W. Wolfendale, *J. Phys. G: Nucl. Part. Phys.* **27**, 1005 (2001).
51. H. Völk and V. Zirakashvili, in *Proc. 28th Int. Cosmic Ray Conf., Tsukuba* **4**, 2031 (2003).
52. S. Ogio and F. Kakimoto, in *Proc. 28th Int. Cosmic Ray Conf., Tsukuba* **1**, 315 (2003).
53. E. Roulet, *Int. J. Mod. Phys.* **A19**, 1133 (2004).
54. A. A. Lagutin *et al.*, *Nucl. Phys. B (Proc. Suppl.)* **97**, 267 (2001).
55. S. Karakula and W. Tkaczyk, *Astropart. Phys.* **1**, 229 (1993).
56. M. T. Dova *et al.*, preprint astro-ph/0112191 (2001).
57. J. R. Hörandel, *Astropart. Phys.* **21**, 241 (2004).
58. R. D. Blanford and J. P. Ostriker, *Astrophys. J.* **221**, L29 (1978).
59. R. Wigmans, *Astropart. Phys.* **19**, 379 (2003).
60. J. Candia *et al.*, *Astropart. Phys.* **17**, 23 (2002).
61. S. Hannestad, *New J. Phys.* **6**, 108 (2004).
62. D. Kazanas and A. Nicolaidis, *Gen. Rel. Grav.* **35**, 1117 (2001).
63. A. A. Petrukhin, *Phys. Atom. Nucl.* **66**, 517 (2003).
64. R. Wischnewski *et al.*, *Int. J. Mod. Phys. A*, in press (2005).